Title

Performance of Spherical Quantum Well Down Converters in Solid State Lighting

Journal

ACS Applied Materials & Interfaces, 13(10)

ISSN

1944-8244

Authors

Rreza, Iva

Yang, Haoran

Hamachi, Leslie

et al.

Publication Date

2021-03-17

DOI

10.1021/acsami.0c15161

Peer reviewed

Performance of Spherical Quantum Well Down Converters in Solid State Lighting

Iva Rreza,[†] Haoran Yang,[‡] Leslie Hamachi,[†§] Michael Campos,[†] Trevor Hull,[†] Joseph Treadway,[%] Juanita Kurtin,[%] Emory Chan,[‡] Jonathan S. Owen*[†]

[†]Department of Chemistry, Columbia University, New York, New York, 10027
[‡]Molecular Foundry, Lawrence Berkeley National Laboratory, Berkeley, California 94720
[§]Department of Chemistry and Biochemistry, California Polytechnic State University, San Luis Obispo, California, 93407

[%]Pacific Light Technologies, Portland, Oregon, 97201

* jso2115@columbia.edu

KEYWORDS solid state lighting, quantum dots, barrier layer, down converters, quantum well

ABSTRACT: We report the color conversion performance of amber and red emitting quantum dots on InGaN solid state lighting (SSL) light emitting diode (LED) packages. Spherical quantum well (SQW) architectures (CdS/$CdSe_{1-x}S_x$/CdS) were finely adjusted using a library of thio- and selenourea synthesis reagents and high throughput synthesis robotics. CdS/$CdSe_{1-x}S_x$ particles with narrow luminescence bands were coated with thick CdS shells (thickness = 1.4 – 7.5 nm) to achieve photoluminescence quantum yields (PLQY) up to 88% at amber and red emission wavelengths (λ_{max} = 600 – 642nm, FWHM < 45 nm). The photoluminescence from SQWs encapsulated in silicone and deposited on LED packages was monitored under accelerated aging conditions (oven temperature = 85 ˚C, relative humidity = 5 – 85%, blue optical power density = 3 – 45 W/cm^2) by monitoring the red photon output over several hundred hours of continuous operation. Growth of a ZnS shell on the SQW surface increases the stability under long-term operation but also reduces the PLQY, especially of SQWs with thick CdS shells. The results illustrate that the outer ZnS shell layer is key to optimizing the PLQY and the long-term stability of QDs during operation on SSL packages.

INTRODUCTION

Improved downconversion materials with narrow band red emission spectra, strong blue absorption, and high chemical stability are needed to increase the efficacy of solid state lighting (SSL).[1] Narrow band red emission is critical to the color rendering index (CRI) and luminous efficacy of radiation (LER) of color converted light emitting diodes (LEDs) with a warm color correlated temperature. Typically, higher CRI and LER lead to lower overall luminous efficacy, but with narrow band red emitters, high efficacy high CRI devices can be achieved. Improvements in these performance parameters can have a significant impact on the adoption of SSL in retail, office, and home lighting applications.[2]

Quantum Dots (QDs) are widely acknowledged as a cost effective front runner among developing downconverters because they emit narrow band luminescence (full width half maximum (*fwhm*) < 30nm) that is tunable across the visible spectrum with a high photoluminescence quantum yield (PLQY).[3] QDs deposited on LED chips have been shown to improve the luminous efficacy of commercial LED packages by 5–18% in devices with high CRI (90).[4] Even greater improvements in the LER are possible if the emission spectral linewidth and photoluminescence quantum yield (PLQY) can be improved.[1] However, QD performance suffers in the demanding environment found on LED packages (“on chip”), which has proven a significant stumbling block to their adoption. The extreme light fluxes (up to 150 W/cm^2) and operating temperatures (up to 150 ˚C) of high-power commercial lighting applications cause photochemical instability of most LED components – including the silicone

encapsulants, conventional phosphors, or QDs – which decreases LED operating lifetime. [5-7,8]

A variety of structural features dictate the performance of QDs under the high intensity illumination found in solid state lighting and lasing applications. In particular structures that accommodate strain, such as core-shell nanoplatelets,[9] and structures that minimize Auger recombination increase the PLQY of biexcitons and trions, such as giant core-shell QDs and graded alloys have been studied.[10-14] Structures that minimize reabsorption are also of interest including those with shells that absorb the blue pump energy. A recently reported CdS/CdSe/CdS spherical quantum well (SQW) architecture achieves these structural features in the same material and achieves near unity PLQY (Figure 1). [15] By growing a thin CdSe layer in between a CdS core and outer CdS shell (i.e. core/shell-1/shell-2), the strain can be mitigated and the outer CdS shell thickness can be increased without compromising the PLQY. Similar shell thicknesses in a CdSe/CdS core/shell QD often results in lower PLQY,[16] but not in all cases.[7, 17] We recently published a synthetic method that can tailor the architectures of core shell quantum dots in a single synthetic step, and precisely grade the composition of interfaces.[18] Using this synthetic approach we sought to test the down conversion performance of QDs with thick CdS shells and alloyed interfaces under the intense illumination found "on chip" in SSL.

RESULTS AND DISCUSSION

Synthesis and high throughput screening. $CdS/CdSe_{1-x}S_x/CdS$ SQW architectures were synthesized using a recently reported single step synthetic method (Figure 1).[18] The composition of $CdS/CdSe_{1-x}S_x$ core/shell-1 QDs was controlled by injecting a pair of thio- and selenoureas into cadmium oleate solution, or into a solution of cadmium oleate and CdS seeds. The relative conversion reactivity of the thio- and selenoureas determines whether an abrupt core-shell or graded alloy architecture is obtained. These QDs are then shelled with thick outer CdS and ZnS layers and subsequently deposited on LED packages within a silicone encapsulant.

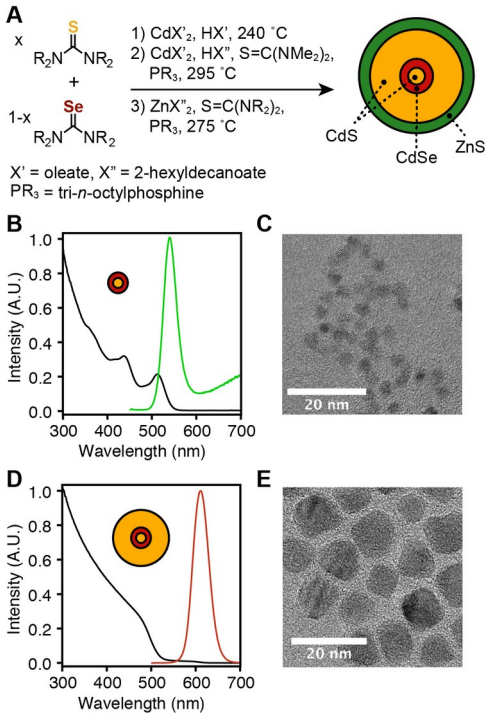

Figure 1. Synthesis of SQWs evaluated in this study. (A) Combining thio- and selenoureas with desired reactivity creates a core and first shell, that is subsequently coated with CdS and ZnS shells prior to encapsulation in silicone on an LED package. (B and C) Example CdS/CdSe core/shell-1, UV-Visible absorption (black) and photoluminescence (green) spectra and TEM, illustrating the narrow absorption and emission features and relatively monodisperse core/shell-1 materials. (D and E) Spectra and TEM following syringe pump addition of CdS shell.

The number, type, and ratios of precursors creates a diverse range of possible outcomes that was searched using high throughput robotics. Precursor concentrations and ratios, reaction temperatures, reaction times, and surfactants were surveyed to identify desirable photoluminescence wavelengths and linewidths.[13] Figure 2 shows the photoluminescence wavelength maximum and *fwhm* of more than 1000 aliquots taken during the synthesis of $CdS/CdSe_{1-x}S_x$ core/shell-1 particles under more than 150 different conditions. In many cases, broad photoluminescence features derive from overlapping emission bands that signal multiple QD populations as was described previously.[18]

Syntheses that provide narrow emission linewidths in the green and yellow spectral regions (540–575nm) were selected for shelling with CdS using a syringe pump method. Deposition of the CdS shell red-shifts the photoluminescence to a wavelength that is desirable for SSL devices with high CRI (λ_{max} = 625). Addition of a CdS shell was achieved by slow addition of cadmium oleate, tetramethylthiourea, and tri-*n*-octylphosphine into a solution of crude CdS/CdSe core/shell-1 nanocrystal synthesis mixture at 290 ˚C (Figure

3). Growth of the shell leads to a steady red shift of the luminescence band and an increase in the PLQY to as high as 88% as the shells thicken (Table 1).

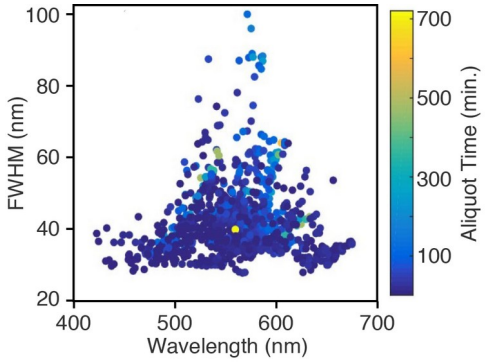

Figure 2. Photoluminescence wavelength and FWHM of aliquots from CdS/$CdSe_{1-x}S_x$ heterostructure syntheses surveying precursor combinations, ratios, temperatures, etc.. The color of the symbols represents the time at which the aliquots were taken as show in the legend.

Interestingly, at lower temperatures and when tri-*n*-octylphosphine is excluded, shell growth continues up to ~6 nm in total diameter, after which the QDs undergo irreversible aggregation. Addition of tri-*n*-octylphosphine and increasing the shelling temperature prevents precipitation and allows thicker shells to be grown. These changes also induce a change from a zincblende to a wurtzite crystal structure analogous to a previous report (Figure S1).[9] Control experiments showed that both the high temperature and the presence of tri-*n*-octylphosphine are required to cause the phase change. A quasi-octahedral crystal habit is formed as the QDs grow beyond 15 nm (Figure 1 and S1).

Sample (X)	Total D.[a] (nm)	Size Core Radius/ Shell-1/Shell-2 (nm)	λ_{em} (nm)	fhwm (nm)	PLQY[b] (%)
1a (Se[c])	6.2	0.7/0.8/1.6	600	40	62
1b (Se[c])	8.8	0.7/0.8/2.9	608	39	83
1c (Se[c])	10	0.9/1.2/2.9	623	36	72
1d (Se[c])	9.4	0.7/0.8/3.2	619	41	81
1e (Se[c])	10.9	0.7/0.8/3.95	611	42	81
1f (Se[c])	16	0.9/1.2/5.9	642	42	84
1g (Se[c])	19.1	0.9/1.2/7.45	625	32	88
2a ($S_{0.1}Se_{0.9}$[d])	9	1.15/0.85/2.5	620	43	78
2b ($S_{0.2}Se_{0.8}$[d])	9.7	1.15/1/2.7	627	41	86
2c ($S_{0.1}Se_{0.9}$[d])	10.3	1.15/1/3	633	39	64
2d ($S_{0.1}Se_{0.9}$[d])	12	1.15/0.85/4	627	43	83
2e ($S_{0.1}Se_{0.9}$[d])	14.5	1.15/0.85/5.25	635	41	75
2f ($S_{0.1}Se_{0.9}$[d])	18.2	1.15/0.85/7.1	636	46	42

Table 1. Summary of quantum well (CdS/$CdSe_{1-x}S_x$/CdS) parameters that underwent on chip performance testing.

[a] *Total diameter values are measured using TEM across the diagonal of particle shape and are averages of 200–300 particles.* [b]*Solution PLQY* [c] *Single injection synthesis of CdS/CdSe core/shell-1 beginning with Se-Im(iPr₂) and N-hexyl, N'-dodecyl thiourea. The C/S dimensions are estimated from the ratio of precursors assuming 100% yield.* [d]*CdS seeds injected with Se-Im(t-Bu₂), S-Im(H,Ph) precursors. Following each step of the reaction, the dimensions of the shell layers are measured using TEM across the diagonal of particle shape and are averages of 200–300 particles.*

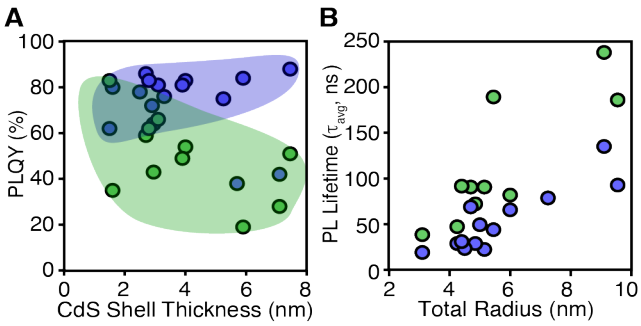

Figure 3. The relationship between (A) PLQY (%), (B) average solution photoluminescence lifetime (τ_{avg}), as a function of the CdS shell thickness before (blue data points) and after ZnS shelling (green).

Spectroscopic Analysis of SQWs. Biexciton photoluminescence quantum yields (BXQY) of CdS/CdSe/CdS SQWs were measured using a photon antibunching method. The ratio of photons emitted from biexcitons and single excitons and/or trions (BWQY/SXQY) can be estimated from the photoluminescence correlation function of single SQWs measured on a scanning confocal photoluminescence microscope in a Hanbury Brown Twiss configuration.[19] Thicker CdS shells and larger CdSe cores are known to increase the BXQY/SXQY of CdSe/CdS QDs, however, thicker shells can also reduce the PLQY of CdSe/CdS QDs.[14, 20-21] The PLQY of the SQWs, on the other hand, slightly increases as the shell thickens, which is consistent with the previous report (Figure 3).[15] Antibunching measurements on single SQWs show that the BWQY/SXQY reaches values as high as 30% as the shell reaches 3.9 nm in thickness (Figure S2). The BXQY of QDs with thinner shells shows nearly complete antibunching from which

we estimate BXQY less than 1%. These trends are consistent with the well-known scaling of the Auger recombination with the QD volume[22] and verify that SQWs of increasingly large volumes have reduced Auger recombination and increased PLQY. Both can increase the down conversion performance under high intensity illumination on SSL packages. Together with the strong absorption in the blue spectral region, low absorption in the green and red regions, a thick CdS shell is highly desirable for solid state lighting applications. However, such architectures had some of the lowest performance on SSL packages in this study.

ZnS shells were deposited on the SQWs following previous reports.[4-5] Growth of ZnS and encapsulation reduces the PLQY, especially of SQWs with thick CdS shells (Figure 3A). A drop in the PLQY following growth of ZnS on II-VI QDs is well documented and typically attributed to interfacial strain between the ZnS layer and underlying substrate material when the ZnS shells grows beyond the critical thickness (~3 nm).[23-33] Similarly, strain is thought to induce the nucleation of ZnS islands that roughen the ZnS surface.[24, 33] Patchy and irregular ZnS shells are typical of the QDs prepared here, particularly when depositing on larger SQWs (Figure S3 and S4). Increased strain at the CdS/ZnS interface in larger SQWs may explain the size dependence of the PLQYs shown in Figure 3.

As the outer CdS shell is added to $CdS/CdSe_{1-x}S_x$ QDs, a systematic increase in the average photoluminescence lifetime (τ_{avg}) beyond 100 nanoseconds is observed, much like the behavior of other CdSe/CdS heterostructures.[34] Addition of the ZnS shell further lengthens the τ_{avg} to as much as 2 µsec (Table S1). Given the large difference in the conduction band offsets at the CdS/ZnS interface and the drop in the PLQY, the longer photoluminescence lifetimes following ZnS deposition may be attributed to the "delayed photoluminescence" following a trapping/detrapping process prior to radiative recombination.[26, 35] The very strong influence of the ZnS layer on the PLQY and lifetime, especially of the largest QDs, suggest that optimizing the ZnS layer and its compatibility with the underlying core is essential to achieve high performance QDs for SSL.

Performance Testing on LED Packages. QDs were dispersed in silicone resins, deposited on LED packages or on quartz discs, cured, and tested following previously published methods.[5] Without a ZnS shell, encapsulation quenches the PLQY; from 62% in solution to <5% in one example. ZnS shells help preserve the PLQY, particularly for smaller QDs, where PLQYs greater than 50% following encapsulation were achieved (Figure 4A). The temperature dependence of the PLQY was measured by heating silicone encapsulated QDs to 140 ˚C on a hot plate and monitoring the PLQY as the film cools (Figure 4 and S5). The depression of PLQY at high temperatures is well-known and largely reversible provided the QDs have a core/shell structure and the temperature is maintained below ~100 ˚C.[36-38] In all cases, the temperature dependence and reliability of the QDs could be predicted by their PLQY at room temperature. Those QDs with the lowest PLQY at room temperature had the lowest PLQYs at 120 ˚C, a representative operating temperature of a mid-power SSL package (Figure S5).

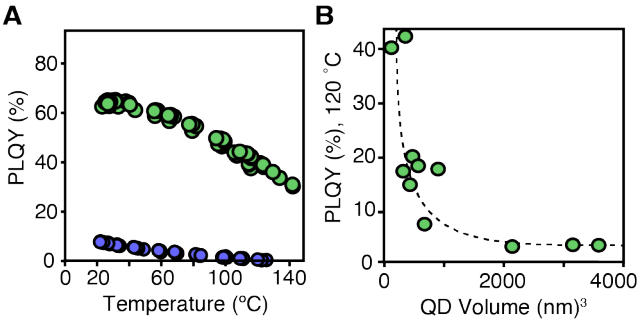

Figure 4. (A) PLQY of d = 6.2 nm CdS/CdSe/CdS (**1a**, 0.7/0.8/1.6 nm) SQW in silicone, as a function of temperature with ZnS shell (green), and without ZnS shell (blue trace). See Figure S5 for performance of other SQWs. (B) PLQY in silicone at 120 ˚C vs QD volume. Dashed black line (r^{-1}) included as a guide to the eye.

The operating lifetime of QDs on mid-power SSL packages were assessed at < 5% relative humidity and a drive current of 240 or 480 mA. This is 4–8 times greater than typical drive currents for these packages, producing radiative power densities of 22 or 45 W/cm^2 at the chip surface and operating temperatures of 85–100 ˚C as was measured by the wavelength shift of the photoluminescence under operation. The intensity of red photons from the QDs is monitored over more than 1000 hours of continuous operation (Figure 5). During this period, the PLQY decreases and the λ_{max} of the photoluminescence blue shifts slightly, changes that may reflect degradation of the QD shelling material. Despite the drop in PLQY following growth of a ZnS shell, the long-term reliability "on chip" is greatly improved compared to QDs without ZnS shells. Without a ZnS shell, the optical output is 3-5 times less intense and drops near zero within 500 hours. ZnS shelled SQWs maintained a moderate, albeit slowly decreasing PLQY over several hundred hours. Over that time, the PLQY typically drops to 50% of the starting PLQY (Figure S7). Under humid conditions (85 % relative humidity), the decrease is more rapid.

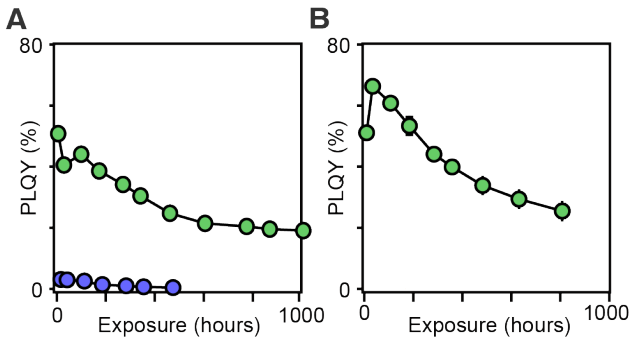

Figure 5. PLQY of red QD luminescence on SSL packages (d = 6.2 nm CdS/CdSe/CdS (**1a**, 0.7/0.8/1.6 nm)). (A) high temperature operating lifetime test (100℃, <5% RH, 240mA,) with (green) and without (blue) ZnS passivation. (B) wet high temperature operating lifetime test (85℃, 85% RH, 65mA) with ZnS passivation.

The presence of a ZnS shell is integral to the performance and reliability of QDs dispersed in silicones on chip. Methods that maintain the PLQY following ZnS deposition are essential to reaching higher performance QD enhanced SSL. This reduction is greater in the largest QDs studied here, eroding the potential benefits of the reduced Auger recombination kinetics of thick shell, or graded alloy architectures. The anti-correlation with CdS shell thickness suggests a strain induced trapping mechanism may limit the performance. Nanostructures that mitigate strain at the CdS/ZnS interface, including graded alloys, nanoplatelets, and quantum well architectures may be better suited to SSL applications. Improvements to the ZnS surface passivation and more detailed understanding of the source of PLQY loss following ZnS growth may also improve long term reliability on chip.

CONCLUSION

The on chip down conversion reliability of amber and red spherical quantum wells of varying CdS shell thickness and alloyed interfaces were studied. Although QDs with PLQYs as high as 88%, and BXQYs as high as 32% could be obtained in samples with thick outer CdS shells, this solution performance did not translate to high PLQY on chip. In particular, the high PLQY of the larger SWQs is eroded by a ZnS surface layer that is required for reliable operation following dispersal in the silicone encapsulant. The ZnS shells allowed several QDs studied here to maintain 50% of their initial performance after 1000 hours of operation under accelerated ageing tests. We conclude that improved surface coatings that preserve the PLQY and maintain reliable performance on chip are essential to the on chip application of QD down converters.

EXPERIMENTAL

General Considerations. All reactions were run using standard air-free techniques and purification was done in air. Toluene (99.5%), methyl acetate (99%), hexanes (98.5%), acetone (99.8%), tetramethylthiourea (98%), triethyl orthoformate (98%), trifluoroacetic anhydride (99%), trifluoroacetic acid (99%), oleic acid (99%) and selenium powder -100 mesh (99.99%) were obtained from Sigma Aldrich and used without purification. Cadmium oxide (99.99%) was obtained from Strem and used without further purification. 1-octadecene (90%) and tetraethylene glycol dimethyl ether (“tetraglyme”, 99%) were obtained from Sigma Aldrich, stirred with calcium hydride overnight, and distilled prior to use. 2-Hexyldecanoic acid (96%) was obtained from Sigma Aldrich, stirred with sodium sulfate overnight, and distilled prior to use. Cadmium oleate, 1,3-diphenylimidazolidene-2-selenone (*Se*-Im(Ph_2), 1,3-*tert*butylimidazolidene-2-selenone (*Se*-Im(t-Bu_2)), N-hexyl-N’-dodecylthiourea, 1,3-diethylimidazolidene-2-selenone (*Se*-Im(Et_2)) 1,3-diisopropyllimidazolidene-2-thione (*Se*-Im(iPr_2)), 1-phenylimidazolidene-2-thione (*S*-Im(H,Ph)) were synthesized and purified according to previously reported methods.[11]

UV−Vis spectra were obtained using a PerkinElmer Lambda 950 spectrophotometer equipped with deuterium and halogen lamps. Powder X-ray diffraction (XRD) was measured on a PANalytical X'Pert Powder X-ray diffractometer. Photoluminescence measurements were performed using a Fluoromax 4 from Horiba Scientific, and PLQYs were determined using a quanta-phi integrating sphere accessory according to a previously described procedure.[15] Transmission Electron Microscopy was done using an FEI Talos F200X instrument. High throughput UV/visible absorption and PL spectra of diluted aliquots were measured in a 96-well quartz microplate (Hellma) using a Biotek Synergy4 microplate reader.

Spherical Quantum Well Synthesis. Spherical quantum wells are prepared through a syringe pump shelling of CdS/$CdSe_{1-x}S_x$ core/shell-1. The CdS/$CdSe_{1-x}S_x$ particles are synthesized either by a one-pot single injection or deposition of $CdSe_{1-x}S_x$ onto previously-isolated CdS QDs.[1118]

High-throughput screening of CdS/$CdSe_{1-x}S_x$ core synthesis. The high-throughput synthesis and analysis was carried out on WANDA (Workstation for Automated Nanomaterial Discovery and Analysis),[39] in a nitrogen filled glovebox. In a typical procedure, eight 40 ml vials are each loaded with cadmium oleate (0.12 mmol, 0.081 g), oleic acid (90%, 0.24 mmol, 0.068 g), designated amount (0 to 5 mL) of 2.8 nm CdS seed solution, and designated amount 1-octadecene to make a total volume of 10 mL. The eight vials are then loaded into the reactor sleeves. Meanwhile, chalcogen precursor solutions of 0.2 M are made by dissolving the thiourea and selone compounds in desired ratios in tetraglyme in 8 mL vials at 100 °C on the robot deck. The robot is programmed to execute the eight reactions in a sequential manner, and each of the reactions is controlled separately. For each reaction, the cadmium oleate solution is heated to the target temperature at a rate of 30 °C/min under a magnetic stirring rate of 500 rpm. The temperature is allowed to stabilize for 5 min upon reaching the desired value. Then, 1 mL of the chalcogen precursor is injected at a rate of 1.5 mL/s to the cadmium oleate solution and left to react for designated timespan. During the reaction, 8 to 12 aliquots are withdrawn from the reaction solution at the programmed time, and loaded into clean 2 mL vials for future analysis. The reaction was then quenched by rapidly cooling the vial with a nitrogen gas flow. When the temperature drops below 50 °C, the reaction is considered complete and the next reaction in the

sequence is automatically begun until the full sequence of reactions is complete.

Example synthesis of CdS/CdSe *cores.* 1) *CdS/CdSe core QDs, λ_{em} = 554 nm, FWHM: 36 nm*. In a nitrogen-filled glovebox, a 100 mL 3-neck round bottom flask is charged with cadmium oleate (0.121 mmol, 0.082 g), oleic acid (0.242 mmol, 0.062 g) and 1-octadecene (9.5 mL, 7.496 g) and sealed with rubber septa. Separately, tetraglyme (0.5 mL, 0.505 g), *N*-hexyl-*N'*-dodecylthiourea (0.020 mmol, 0.0066 g), *Se*-Im(iPr_2) (0.091 mmol, 0.021 g) are combined in a 4 mL vial and the vial is sealed with a rubber septum. The three-neck flask is then transferred to a Schlenk line and heated to 240˚C under argon, after which the chalcogen solution is swiftly injected into the flask. The reaction is run for 7 hours.

Example synthesis of d = 2.3 nm CdS seeds. In a nitrogen filled glovebox, a 100 mL three neck round bottom flask is charged with cadmium oleate (0.19 mmol, 0.122 g), oleic acid (0.36 mmol, 0.102 g), and 1-octadecene (14.25 mL, 11.24 g) and sealed with rubber septa. Separately, tetraglyme (0.75 mL, 0.75 g) and *N-phenyl, N',N'-dibutylthiourea* (0.15 mmol, 0.040 g) are combined in 4 mL vial and the vial is sealed with a rubber septum. The three-neck flask is then transferred to a Schlenk line and heated to 240˚C under argon, after which the thiourea solution is swiftly injected into the flask. The reaction is run for 2 minutes before cooling to room temperature. The CdS seed particles are used as synthesized for subsequent seeded growth reactions.

Synthesis of CdS/$CdSe_{0.9}S_{0.1}$ particles λ_{em} = 576 nm, FWHM: 37.9 nm. In a nitrogen-filled glovebox, a 100 mL three neck round bottom flask is charged with cadmium oleate (0.18 mmol, 0.122 g), oleic acid (0.36 mmol, 0.102 g), a solution of CdS particles with *d* = 2.3 nm (0.85 mL) and 1-octadecene (14.25 mL, 11.24 g) and sealed with rubber septa. Separately, tetraglyme (0.75 mL, 0.75 g), *S*-Im(H,Ph) (0.03 mmol, 0.0053 g), and *Se*-Im(tBu_2) (0.12 mmol, 0.031 g) are combined in 4 mL vial and the vial is sealed with a rubber septum. The three neck flask is then transferred to a Schlenk line and heated to 240˚C under argon, after which the chalcogen solution is swiftly injected into the flask. The reaction is run for 30 minutes.

Synthesis of CdS/$CdSe_{0.9}S_{0.1}$ particles λ_{em} = 595 nm FWHM: 35.8 nm. In a nitrogen filled glovebox, a 100 mL three neck round bottom flask is charged with cadmium oleate (0.18 mmol, 0.122 g), oleic acid (0.36 mmol, 0.102 g), a solution of CdS particles with *d* = 2.3 nm (0.75 mL) and 1-octadecene (14.25 mL, 11.24 g) and sealed with rubber septa. Separately, tetraglyme (0.85 g, 0.85 mL), *S*-Im(H,Ph) (0.017 mmol, 0.003 g), and *Se*-Im(tBu_2) (0.153 mmol, 0.040 g) are combined in 4 mL vial and the vial is sealed with a rubber septum. The three neck flask is then transferred to a Schlenk line and heated to 240˚C under argon, after which the chalcogen solution is swiftly injected into the flask. The reaction is run for 1 hour.

Synthesis of CdS/$CdSe_{0.8}S_{0.2}$ particles λ_{em} = 583 nm, FWHM: 36 nm. In a nitrogen filled glovebox, a 100 mL three neck round bottom flask is charged with cadmium oleate (0.18 mmol, 0.122 g), oleic acid (0.36 mmol, 0.102 g), a solution of CdS particles with *d* = 2.3nm (0.85 mL) and 1-octadecene (14.25 mL, 11.24 g) and sealed with rubber septa. Separately, tetraglyme (0.75 mL, 0.75 g), *S*-Im(H,Ph) (0.03 mmol, 0.0053 g), and *Se*-Im(tBu_2) (0.12 mmol, 0.031 g) are combined in 4 mL vial and the vial is sealed with a rubber septum. The three neck flask is then transferred to a Schlenk line and heated to 240˚C under Ar, after which the chalcogen solution is swiftly injected into the flask. The reaction is run for 30 minutes.

CdS Shell Growth Solution. In a nitrogen-filled glovebox, a 3-neck round bottom flask is charged with a solution of cadmium oleate (4.49 mmol, 3.03 g), 2-hexyldecanoic acid (4.5 mmol, 1.32 mL, 1.155 g), and 1-octadecene (41.25 mL). The solution is transferred to a Schlenk line and heated in an oil bath at 150˚C to obtain a clear homogenous solution. Separately, tetramethyl thiourea (1.5 mmol, 0.198 g) and tetraglyme (2.175 mL, 2.175 g) are combined in a 20mL vial equipped with a stir bar, sealed with a rubber septum, and stirred to obtain a clear colorless solution. Gentle heating (<100˚C) can be applied to speed the dissolution. The room temperature thiourea solution is combined the cadmium oleate solution and mixed.

Example Synthesis of CdS/$CdSe_{1-x}S_x$/CdS*.* A 10 mL solution of CdS/$CdSe_{1-x}S_x$ core QDs prepared as described above is transferred to a 3-neck round bottom and heated to 290 °C. Once the solution reaches temperature, the CdS shell growth solution is injected at 5.0 mL/hr. The shelling reaction is run for an allotted time (see below). The resulting nanocrystals are isolated by precipitation with acetone or isopropyl alcohol (80–150 mL) and centrifuged (7000 rpm, 10 min). The resulting pellet is dispersed in hexane (~25–75ml) and byproducts are precipitated with acetone (~10–20ml). The long reaction times produces polymers of octadecene[40] that can be partially removed following several precipitations from hexane with acetone. The resulting NC solution is decanted, dried under vacuum and resuspended in ~20ml toluene. Three rounds of dissolution in toluene (~10mL) and precipitation with methyl acetate (~30ml) were sufficient to fully purify the NCs.

Synthesis of ***1a***, ***1b***, ***1d***, ***1e*** *λ_{em} = 600 nm, 608 nm, 611 nm, 619 nm.* CdS/CdSe particles (λ_{em} = 554 nm) shelled at 5.0mL/hr for 2 hr, 5.5 hr, 11 hr, and 11.5 hr.

Synthesis of ***1c***, ***1f***, ***1g*** *λ_{em} = 623 nm, 642 nm, 625 nm.* CdS/CdSe particles (λ_{em} = 577 nm) shelled at 5.0mL/hr for 24hr (**1c**), 10mL/r for 15hr (**1f**), 5.0mL/hr for 46hr.

*Synthesis of **2a**, **2d**, **2e**, **2f** λ_{em} = 620 nm, 627 nm, 635 nm, 636nm.* CdS/$CdSe_{0.9}S_{0.1}$ (λ_{em} = 575 nm) shelled at 4.5 mL/hr for 16 hr, 26 hr, 36 hr, and 43 hr.

*Synthesis of **2c** λ_{em} = 633 nm.* CdS/$CdSe_{0.9}S_{0.1}$ particles (λ_{em} = 594 nm) shelled at 1.5 mL/hr for 16 hr.

*Synthesis of **2b** λ_{em} = 627 nm.* CdS/$CdSe_{0.8}S_{0.2}$ particles (λ_{em} = 583 nm) shelled at 2.5 mL/hr for 18 hr.

Biexciton Quantum Yield Measurements. Single QD photoluminescence measurements were performed on a time correlated single photon counting (TCSPC) Picoquant Microtime200 confocal fluorescence microscope using Symphotime64 software. Samples were excited using a 405nm pulsed laser with tunable rep rate. Photoluminescence was collected through a 100x objective, past a dichroic mirror, and through a 50 µm pinhole before being split onto two silicon single photon avalanche diodes via a 50/50 beam splitting cube. Photon arrival times after the laser pulse were histogrammed to form PL lifetime decays. Photon arrival times since the experiment start were cross-correlated between the two detectors to form antibunching curves.[41-42] Only single nanoparticles, determined using time-gating software techniques,[43] were used for analysis. All samples were excited at 1 MHz in the low power regime (average 40nW, 40 mW/cm^2) used by Nair et al.[19] QDs were spun onto #1 glass substrates with 0.05 wt% PMMA to increase the yield of single QDs. Background noise contributed less than 10% of signal, based on previous estimates[19], but was not subtracted. Avalanche breakdown flash, seen in other previous antibunching studies[43] was taken into consideration when estimating low BXQY values.

Encapsulation and accelerated ageing tests. QDs were encapsulated and deposited on LED packages following previously reported methods.[5] Silicone slurry mixtures with QDs were cured on LED chips (2.4 mm^2, 30/30 packages). High temperature operating lifetime tests are performed with a driving current of either 240 mA or 480 mA at 100 ˚C and ambient humidity (<5% relative humidity). Humid, high temperature lifetime tests are performed with a driving current of 30 mA at 85 ˚C and 85 % relative humidity. The thermal droop profiles are obtained by heating a cured QD silicone film atop a glass slide to desired temperature and collecting quantum yields during cool down.

ASSOCIATED CONTENT

Supporting Information

The Supporting Information is available free of charge on the ACS Publications website. Powder x-ray diffraction, transmission electron microscopy, photon antibunching, temperature dependent PLQY and reliability testing of QDs is provided in the supporting information (PDF).

AUTHOR INFORMATION

Corresponding Author

* Department of Chemistry, Columbia University, New York, NY 10027.

Present Addresses

†Department of Chemistry, Columbia University, New York, New York, 10027

‡ Molecular Foundry, Lawrence Berkeley National Laboratory, Berkeley, CA 94720

Author Contributions

The manuscript was written through contributions of all authors.

ACKNOWLEDGMENT

This work was supported by the Solid State Lighting Program, of the Office of Energy Efficiency and Renewable Energy, Department of Energy under project: DE-EE0007628. Work at the Molecular Foundry was supported by the Office of Science, Office of Basic Energy Sciences, of the U.S. Department of Energy under Contract No. DE-AC02-05CH11231. Scanning confocal photoluminescence microscropy was support by the U.S. Army under contract W911NF-16-1-0211.

ABBREVIATIONS

BXQY, biexciton photoluminescence quantum yields; CRI, color rendering index; LED, light emitting diode; LER, luminous efficacy of radiation; QD, quantum dot; SSL, solid state lighting; SQW, spherical quantum well; TCSPC, time correlated single photon counting;

REFERENCES

1. Pattison, P. M.; Hansen, M.; Tsao, J. Y., LED lighting efficacy: Status and directions. *Cr Phys* **2018,** *19* (3), 134-145.
2. Multi-Year Program Plan FY'09-FY'15 Solid-State Lighting Research and Development. Information, O. o. S. a. T., Ed. 2009.
3. Pattison, M.; Hansen, M.; Bardsley, N.; Elliot, C.; Lee, K.; Pattison, L.; Tsao, J. Y., 2019 Lighting R&D Opportunities. U.S. Department of Energy, O. o. R. E., Ed. 2019.
4. Mangum, B. D.; Landes, T. S.; Theobald, B. R.; Kurtin, J. N., Exploring the bounds of narrow-band quantum dot downconverted LEDs. *Photon. Res.* **2017,** *5* (2), A13-A22.
5. Shimizu, K. T.; Bohmer, M.; Estrada, D.; Gangwal, S.; Grabowski, S.; Bechtel, H.; Kang, E.; Vampola, K. J.; Chamberlin, D.; Shchekin, O. B.; Bhardwaj, J., Toward commercial realization of quantum dot based white light-emitting diodes for general illumination. *Photon. Res.* **2017,** *5* (2), A1-A6.

6. Orfield, N. J.; Majumder, S.; Hu, Z.; Koh, F. Y.-C.; Htoon, H.; Hollingsworth, J. A., Kinetics and Thermodynamics of Killing a Quantum Dot. *ACS Applied Materials & Interfaces* **2020,** *12* (27), 30695-30701.
7. Orfield, N. J.; Majumder, S.; McBride, J. R.; Yik-Ching Koh, F.; Singh, A.; Bouquin, S. J.; Casson, J. L.; Johnson, A. D.; Sun, L.; Li, X.; Shih, C.-K.; Rosenthal, S. J.; Hollingsworth, J. A.; Htoon, H., Photophysics of Thermally-Assisted Photobleaching in "Giant" Quantum Dots Revealed in Single Nanocrystals. *Acs Nano* **2018,** *12* (5), 4206-4217.
8. He, Z.; Zhang, C.; Chen, H.; Dong, Y.; Wu, S.-T., Perovskite Downconverters for Efficient, Excellent Color-Rendering, and Circadian Solid-State Lighting. *Nanomaterials* **2019,** *9* (2).
9. Mahler, B.; Nadal, B.; Bouet, C.; Patriarche, G.; Dubertret, B., Core/Shell Colloidal Semiconductor Nanoplatelets. *J Am Chem Soc* **2012,** *134* (45), 18591-18598.
10. Park, Y. S.; Lim, J.; Makarov, N. S.; Klimov, V. I., Effect of Interfacial Alloying versus "Volume Scaling" on Auger Recombination in Compositionally Graded Semiconductor Quantum Dots. *Nano Lett* **2017,** *17* (9), 5607-5613.
11. Bae, W. K.; Padilha, L. A.; Park, Y. S.; McDaniel, H.; Robel, I.; Pietryga, J. M.; Klimov, V. I., Controlled Alloying of the Core-Shell Interface in CdSe/CdS Quantum Dots for Suppression of Auger Recombination. *Acs Nano* **2013,** *7* (4), 3411-3419.
12. Garcia-Santamaria, F.; Chen, Y. F.; Vela, J.; Schaller, R. D.; Hollingsworth, J. A.; Klimov, V. I., Suppressed Auger Recombination in "Giant" Nanocrystals Boosts Optical Gain Performance. *Nano Lett* **2009,** *9* (10), 3482-3488.
13. Pietryga, J. M.; Park, Y. S.; Lim, J. H.; Fidler, A. F.; Bae, W. K.; Brovelli, S.; Klimov, V. I., Spectroscopic and Device Aspects of Nanocrystal Quantum Dots. *Chem Rev* **2016,** *116* (18), 10513-10622.
14. Park, Y. S.; Bae, W. K.; Padilha, L. A.; Pietryga, J. M.; Klimov, V. I., Effect of the Core/Shell Interface on Auger Recombination Evaluated by Single-Quantum-Dot Spectroscopy. *Nano Lett* **2014,** *14* (2), 396-402.
15. Jeong, B. G.; Park, Y.-S.; Chang, J. H.; Cho, I.; Kim, J. K.; Kim, H.; Char, K.; Cho, J.; Klimov, V. I.; Park, P.; Lee, D. C.; Bae, W. K., Colloidal Spherical Quantum Wells with Near-Unity Photoluminescence Quantum Yield and Suppressed Blinking. *Acs Nano* **2016,** *10* (10), 9297-9305.
16. Chen, Y.; Vela, J.; Htoon, H.; Casson, J. L.; Werder, D. J.; Bussian, D. A.; Klimov, V. I.; Hollingsworth, J. A., "Giant" multishell CdSe nanocrystal quantum dots with suppressed blinking. *J Am Chem Soc* **2008,** *130* (15), 5026-5027.
17. Tan, R.; Yuan, Y.; Nagaoka, Y.; Eggert, D.; Wang, X.; Thota, S.; Guo, P.; Yang, H.; Zhao, J.; Chen, O., Monodisperse Hexagonal Pyramidal and Bipyramidal Wurtzite CdSe-CdS Core–Shell Nanocrystals. *Chem Mater* **2017,** *29* (9), 4097-4108.
18. Hamachi, L. S.; Yang, H. R.; Jen-La Plante, I.; Saenz, N.; Qian, K.; Campos, M. P.; Cleveland, G. T.; Rreza, I.; Oza, A.; Walravens, W.; Chan, E. M.; Hens, Z.; Crowther, A. C.; Owen, J. S., Precursor reaction kinetics control compositional grading and size of CdSe1-xSx nanocrystal heterostructures. *Chem Sci* **2019,** *10* (26), 6539-6552.
19. Nair, G.; Zhao, J.; Bawendi, M. G., Biexciton Quantum Yield of Single Semiconductor Nanocrystals from Photon Statistics. *Nano Lett* **2011,** *11* (3), 1136-1140.
20. Mangum, B. D.; Sampat, S.; Ghosh, Y.; Hollingsworth, J. A.; Htoon, H.; Malko, A. V., Influence of the core size on biexciton quantum yield of giant CdSe/CdS nanocrystals. *Nanoscale* **2014,** *6* (7), 3712-3720.
21. Oron, D.; Kazes, M.; Banin, U., Multiexcitons in type-II colloidal semiconductor quantum dots. *Physical Review B* **2007,** *75* (3), 035330.
22. Klimov, V. I., Multicarrier Interactions in Semiconductor Nanocrystals in Relation to the Phenomena of Auger Recombination and Carrier Multiplication. *Annu Rev Conden Ma P* **2014,** *5*, 285-316.

23. McBride, J. R.; Mishra, N.; Click, S. M.; Orfield, N. J.; Wang, F.; Acharya, K.; Chisholm, M. F.; Htoon, H.; Rosenthal, S. J.; Hollingsworth, J. A., Role of shell composition and morphology in achieving single-emitter photostability for green-emitting "giant" quantum dots. *The Journal of Chemical Physics* **2020,** *152* (12), 124713.
24. Ji, B.; Koley, S.; Slobodkin, I.; Remennik, S.; Banin, U., ZnSe/ZnS Core/Shell Quantum Dots with Superior Optical Properties through Thermodynamic Shell Growth. *Nano Lett* **2020,** *20* (4), 2387-2395.
25. Greytak, A. B.; Allen, P. M.; Liu, W.; Zhao, J.; Young, E. R.; Popović, Z.; Walker, B. J.; Nocera, D. G.; Bawendi, M. G., Alternating layer addition approach to CdSe/CdS core/shell quantum dots with near-unity quantum yield and high on-time fractions. *Chem Sci* **2012,** *3* (6), 2028-2034.
26. Jones, M.; Lo, S. S.; Scholes, G. D., Quantitative modeling of the role of surface traps in CdSe/CdS/ZnS nanocrystal photoluminescence decay dynamics. *Proceedings of the National Academy of Sciences* **2009,** *106* (9), 3011.
27. Deka, S.; Quarta, A.; Lupo, M. G.; Falqui, A.; Boninelli, S.; Giannini, C.; Morello, G.; De Giorgi, M.; Lanzani, G.; Spinella, C.; Cingolani, R.; Pellegrino, T.; Manna, L., CdSe/CdS/ZnS Double Shell Nanorods with High Photoluminescence Efficiency and Their Exploitation As Biolabeling Probes. *J Am Chem Soc* **2009,** *131* (8), 2948-2958.
28. Chen, Y.; Vela, J.; Htoon, H.; Casson, J. L.; Werder, D. J.; Bussian, D. A.; Klimov, V. I.; Hollingsworth, J. A., "Giant" Multishell CdSe Nanocrystal Quantum Dots with Suppressed Blinking. *J Am Chem Soc* **2008,** *130* (15), 5026-5027.
29. McBride, J.; Treadway, J.; Feldman, L. C.; Pennycook, S. J.; Rosenthal, S. J., Structural Basis for Near Unity Quantum Yield Core/Shell Nanostructures. *Nano Lett* **2006,** *6* (7), 1496-1501.
30. Xie, R.; Kolb, U.; Li, J.; Basché, T.; Mews, A., Synthesis and Characterization of Highly Luminescent CdSe−Core CdS/Zn0.5Cd0.5S/ZnS Multishell Nanocrystals. *J Am Chem Soc* **2005,** *127* (20), 7480-7488.
31. Talapin, D. V.; Mekis, I.; Götzinger, S.; Kornowski, A.; Benson, O.; Weller, H., CdSe/CdS/ZnS and CdSe/ZnSe/ZnS Core−Shell−Shell Nanocrystals. *The Journal of Physical Chemistry B* **2004,** *108* (49), 18826-18831.
32. Dabbousi, B. O.; Rodriguez-Viejo, J.; Mikulec, F. V.; Heine, J. R.; Mattoussi, H.; Ober, R.; Jensen, K. F.; Bawendi, M. G., (CdSe)ZnS Core−Shell Quantum Dots: Synthesis and Characterization of a Size Series of Highly Luminescent Nanocrystallites. *The Journal of Physical Chemistry B* **1997,** *101* (46), 9463-9475.
33. Ji, B. T.; Panfil, Y. E.; Waiskopf, N.; Remennik, S.; Popov, I.; Banin, U., Strain-controlled shell morphology on quantum rods. *Nat Commun* **2019,** *10*.
34. Hanifi, D. A.; Bronstein, N. D.; Koscher, B. A.; Nett, Z.; Swabeck, J. K.; Takano, K.; Schwartzberg, A. M.; Maserati, L.; Vandewal, K.; van de Burgt, Y.; Salleo, A.; Alivisatos, A. P., Redefining near-unity luminescence in quantum dots with photothermal threshold quantum yield. *Science* **2019,** *363* (6432), 1199-+.
35. Rabouw, F. T.; Kamp, M.; van Dijk-Moes, R. J. A.; Gamelin, D. R.; Koenderink, A. F.; Meijerink, A.; Vanmaekelbergh, D., Delayed Exciton Emission and Its Relation to Blinking in CdSe Quantum Dots. *Nano Lett* **2015,** *15* (11), 7718-7725.
36. Zhao, Y. M.; Riemersma, C.; Pietra, F.; Koole, R.; Donega, C. D.; Meijerink, A., High-Temperature Luminescence Quenching of Colloidal Quantum Dots. *Acs Nano* **2012,** *6* (10), 9058-9067.
37. Rowland, C. E.; Schaller, R. D., Exciton Fate in Semiconductor Nanocrystals at Elevated Temperatures: Hole Trapping Outcompetes Exciton Deactivation. *J. Phys. Chem. C* **2013,** *117* (33), 17337-17343.
38. Orfield, N. J.; Majumder, S.; McBride, J. R.; Koh, F. Y. C.; Singh, A.; Bouquin, S. J.; Casson, J. L.; Johnson, A. D.; Sun, L. Y.; Li, X. Q.; Shih, C. K.; Rosenthal, S. J.; Hollingsworth, J. A.; Htoon, H., Photophysics of Thermally-

Assisted Photobleaching in "Giant" Quantum Dots Revealed in Single Nanocrystals. *Acs Nano* **2018,** *12* (5), 4206-4217.
39. Chan, E. M.; Xu, C. X.; Mao, A. W.; Han, G.; Owen, J. S.; Cohen, B. E.; Milliron, D. J., Reproducible, High-Throughput Synthesis of Colloidal Nanocrystals for Optimization in Multidimensional Parameter Space. *Nano Lett* **2010,** *10* (5), 1874-1885.
40. Dhaene, E.; Billet, J.; Bennett, E.; Van Driessche, I.; De Roo, J., The Trouble with ODE: Polymerization during Nanocrystal Synthesis. *Nano Lett* **2019,** *19* (10), 7411-7417.
41. Laurence, T. A.; Fore, S.; Huser, T., Fast, flexible algorithm for calculating photon correlations. *Opt Lett* **2006,** *31* (6), 829-831.
42. Wahl, M.; Gregor, I.; Patting, M.; Enderlein, J., Fast calculation of fluorescence correlation data with asynchronous time-correlated single-photon counting. *Opt Express* **2003,** *11* (26), 3583-3591.
43. Mangum, B. D.; Ghosh, Y.; Hollingsworth, J. A.; Htoon, H., Disentangling the effects of clustering and multi-exciton emission in second-order photon correlation experiments. *Opt Express* **2013,** *21* (6), 7419-7426.

TOC

Red downconversion performance and reliability on LED packages.